



ELSEVIER

Journal of Structural Geology 26 (2004) 2103–2118

**JOURNAL OF  
STRUCTURAL  
GEOLOGY**

www.elsevier.com/locate/jsg

## Active fault geometry and kinematics in Parnitha Mountain, Attica, Greece

A. Ganas<sup>a,\*</sup>, S.B. Pavlides<sup>b</sup>, S. Sboras<sup>b</sup>, S. Valkaniotis<sup>b</sup>, S. Papaioannou<sup>b</sup>, G.A. Alexandris<sup>b</sup>,  
A. Plessa<sup>a</sup>, G.A. Papadopoulos<sup>a</sup>

<sup>a</sup>*Institute of Geodynamics, National Observatory of Athens, Lofos Nymfon, 11810 Athens, Greece*

<sup>b</sup>*Department of Geology, Aristotle University of Thessaloniki, Thessaloniki 54124, Greece*

Received 3 March 2003; received in revised form 15 December 2003; accepted 24 February 2004

Available online 3 August 2004

### Abstract

The Parnitha mountain range lies between two Quaternary rift systems in central Greece: the Gulf of Corinth Rift and the Gulf of Evia rift. We suggest that the range was formed by footwall uplift on active normal faults striking WNW–ESE and NE–SW. We investigated the scarp appearance, geometry and slip rates of three normal faults bounding this mountain range by field mapping at 1:5000 scale. Active faults studied include the 8.5 km long Fili Fault, the 4.7 km long Maliza Fault and the 4 km long Thrakomakedones Fault. We calculated comparable mean slip rates for all mapped faults (Fili: 0.18 mm/yr, Avlon: 0.2 mm/yr, Thrakomakedones: 0.24 mm/yr); however, we suggest that the WNW–ESE structures are more active during the Late Quaternary because of abundant field evidence of recent movements along slip surfaces (fresh basal stripes and slickenlines). In addition, stress axes analysis shows a N7°E–N25°E (NNE–SSW) oriented, extensional stress field, which is compatible with the focal mechanism of the Athens 1999 earthquake. The fault-slip data from the Parnitha faults show orientations similar to other low-strain areas in central Greece, such as the Gulf of Evia Rift to the north. Our slip rate estimates may explain the low recurrence of large earthquakes in Attica as opposed to high slip rate areas in central Greece such as the neighbouring Gulf of Corinth. © 2004 Elsevier Ltd. All rights reserved.

**Keywords:** Active faults; Kinematics; Fault geometry; Fault slip rate; Central Greece; Attica

### 1. Introduction

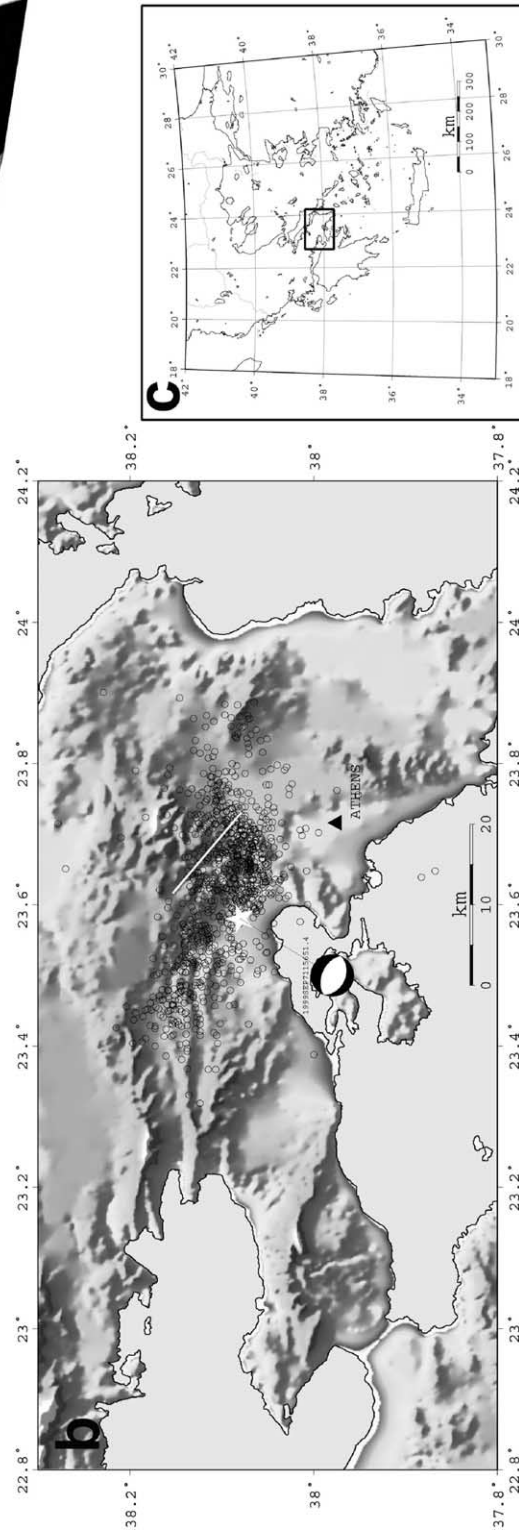
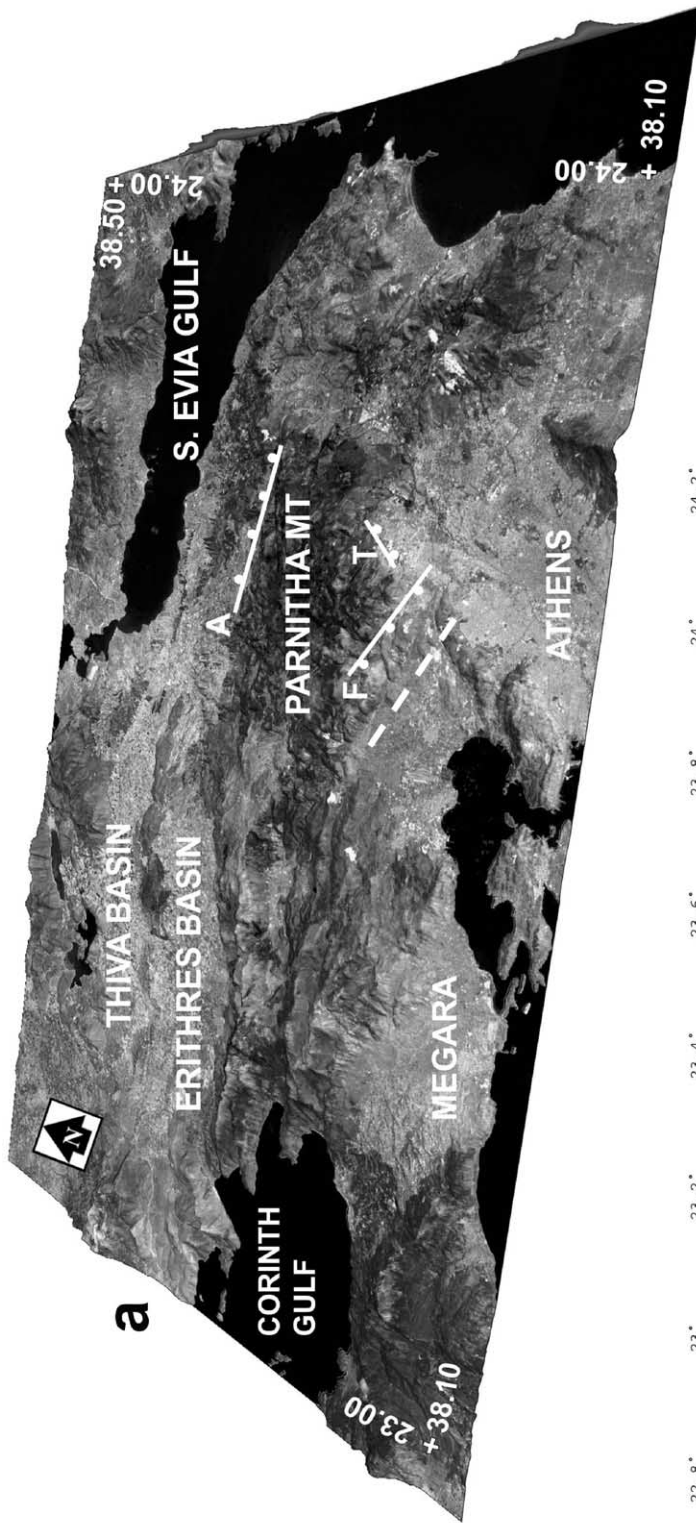
The Parnitha mountain range lies in between two Quaternary rift systems in central Greece: the Gulf of Corinth Rift, and the Gulf of Evia rift (Fig. 1a). The range is up to 1400 m high (HAGS, 1978) and is bounded to the north by the Kaparelli–Oropos fault zone, which produced three large ( $M > 6$ ) earthquakes during the last 110 years (in 1893, 1938 and 1981; Ambraseys and Jackson, 1990; Papadopoulos, 2000; Papadopoulos et al., 2002; see Gulf of Corinth–Erithres basin area in Fig. 1a). In the interior of this range, existing fault maps (e.g. IGME, 1989) show no active structures (faults) or indicate structures with undetermined activity. However, it is in this area that a normal-slip earthquake of  $M_s$  5.9 occurred on September 7th 1999, causing 143 deaths and severe damage in the Athens

Metropolitan area (e.g. Papadopoulos et al., 2000; Pavlides et al., 2002; Fig. 1b).

We examined the neotectonic structure of Parnitha through field mapping during the years 2001–2002. We focused our search for active faults (faults that have moved in the last 130,000 years, i.e. during Late Quaternary times) on the central and southern parts of the range as these regions pose a greater potential threat for Athens. We found that the main faults are located along the foothills of the mountain, in the areas of Thrakomakedones, Fili, and Avlon (see letters T, F, and A in Fig. 1a; Fili is reported as Phyle in the classical literature). A major normal fault bounds the western slopes of Parnitha (Thriassion basin; west of F in Fig. 1a); however, both geological and remote sensing evidence suggest that it is inactive (Ganas et al., 2001; Pavlides et al., 2002). It is possible that other fault scarps showing evidence of Late Quaternary movements may exist towards the interior of the range. Our goal was to locate the prominent ones that are closer to the Athens

\* Corresponding author.

E-mail address: aganas@gein.noa.gr (A. Ganas).



metropolitan area. The main target of detailed geological–neotectonic mapping of selected sites close to normal faults, was to pinpoint exact locations of possible surface faulting. At each of these sites, fault geometry, kinematics and strain pattern (extension directions) were recorded in detail.

Our results are compared with other extensional provinces in central Greece, such as the Gulf of Evia Rift to the North and the Gulf of Corinth Rift to the West (Fig. 1). In particular, we compare our calculations regarding both the stress field orientation and the mean slip rates for all studied faults. The kinematics of the Parnitha faults exhibit important similarities to the low-strain area of the Gulf of Evia. This finding may have important implications for the long-term seismic hazard assessment of the Attica region.

## 2. Geological setting

The pre-rift rocks of Parnitha mainly belong to the SubPelagonian isopic zone of the internal Hellenides. This carbonate platform was developed to the west of the Pelagonian microcontinent (Robertson et al., 1991). The carbonate rocks show mainly neritic facies, spanning the period Triassic–Lower Cretaceous. An early deformation phase occurred during Lower Cretaceous with the emplacement of an ophiolitic suite (Katsikatos, 1977). Large ophiolitic bodies crop out within the SubPelagonian rocks together with typical *mélange* formations as well as chert. The basement consists of Lower Palaeozoic gneisses, mica schists, amphibolites and marble intercalations (Katsikatos et al., 1986). The SubPelagonian rocks have been thrust to the east and south-east on top of the Attico–Cycladic, metamorphic Massif (Pendeli area) during early Tertiary times (e.g. Marinis et al., 1971; Robertson et al., 1991).

Syn-rift rocks include lacustrine marls and marly limestones, sandstones, clays, fluvial conglomerate successions and coastal unconsolidated deposits (Mettos et al., 2000). The date of the synrift ranges from Upper Miocene to Holocene times, i.e. a period of about 10 My. Quaternary rocks also include alluvial fan deposits and steep talus cones. The fan deposits are found at the base of Parnitha where there is a marked break in slope. They are well-stratified conglomerates of water-transported limestone and greywacke pebbles, while the talus deposits are poorly

sorted breccia and are formed by dry transport of individual grains or dry mass flows.

## 3. Field evidence for active faulting

The evidence comprises field data on bedrock scarps juxtaposing pre-rift and synrift rocks, on scarp linearity, scarp height, scarp appearance and fault-slip kinematics that are compatible with the regional stress field (N–S to NNE–SSW; Ambraseys and Jackson, 1990; Kiratzi, 2002; USGS; Fig. 1b). The three normal faults from which we have collected fault-slip data have been mapped at 1:5000 scale. They are generally resistant, striated and corrugated fault-planes developed within Mesozoic carbonates. Slickensides have been measured using a CLAR compass. The main fault planes are typically underlain by several centimetre-to-metre thick fault gouge preserved, at outcrop, within the footwall. These mark the contact between pre-rift rocks (Mesozoic) and synrift rocks (Miocene to Recent). Locally, the fault-planes are characterised by millimetre-scale frictional-wear striae and metre-scale corrugations similar to those described by Hancock and Barka (1987) and Stewart and Hancock (1991). The hanging walls of all three faults are composed of synrift clastic deposits (alluvium or lacustrine sediments with widespread occurrences of slope-derived deposits). Fault-slip data were collected from the main fault planes as these provide information on the kinematics at a time when the faults had sufficient throw to produce a geomorphological escarpment, thus, they were probably mature enough to host large magnitude earthquakes ( $\geq M_s 6.0$ ).

### 3.1. The Fili Fault

The Fili area geological map is shown in Fig. 2 and it covers an area of four 1:5000 map sheets (roughly 8 km E–W by 6 km N–S). The mapped area is included in the 1:50,000 map sheet ‘Elefsis’ (HAGS, 1992), where the main structure is the NW–SE striking Fili normal fault. Our field mapping shows that the fault is segmented into four branches (segments) that are arranged en-*échelon* with right-stepping configuration while maintaining the same strike (N120–N130 degrees) and a dip direction to the SW. The segmentation pattern is visible in high-resolution satellite images (Fig. 3) after suitable contrast enhancement. Despite the small pixel size of the image (5.8 m), the fault

Fig. 1. (a) Oblique view of a satellite image of Attica, central Greece, showing main physiographic features including mountain ranges (dark grey areas), marine gulfs (black areas) and sedimentary basins (light grey areas). Thin white lines with ticks represent active normal faults that were studied during this study (F: Fili, A: Avlon–Maliza, T: Thrakomakedones). Image dimensions: 87 km along E–W, 60 km along N–S. (b) Nadir, shaded relief view of a 250-m digital elevation model (DEM) with low-angle illumination from the north-east. Open circles are epicentres of aftershocks of the Athens 1999 earthquake. The USGS focal mechanism of the main event is also shown as beachball. White line indicates position of the seismic fault after Pavlides et al. (2002). (c) Map of Greece with inset box showing the location of the study area.

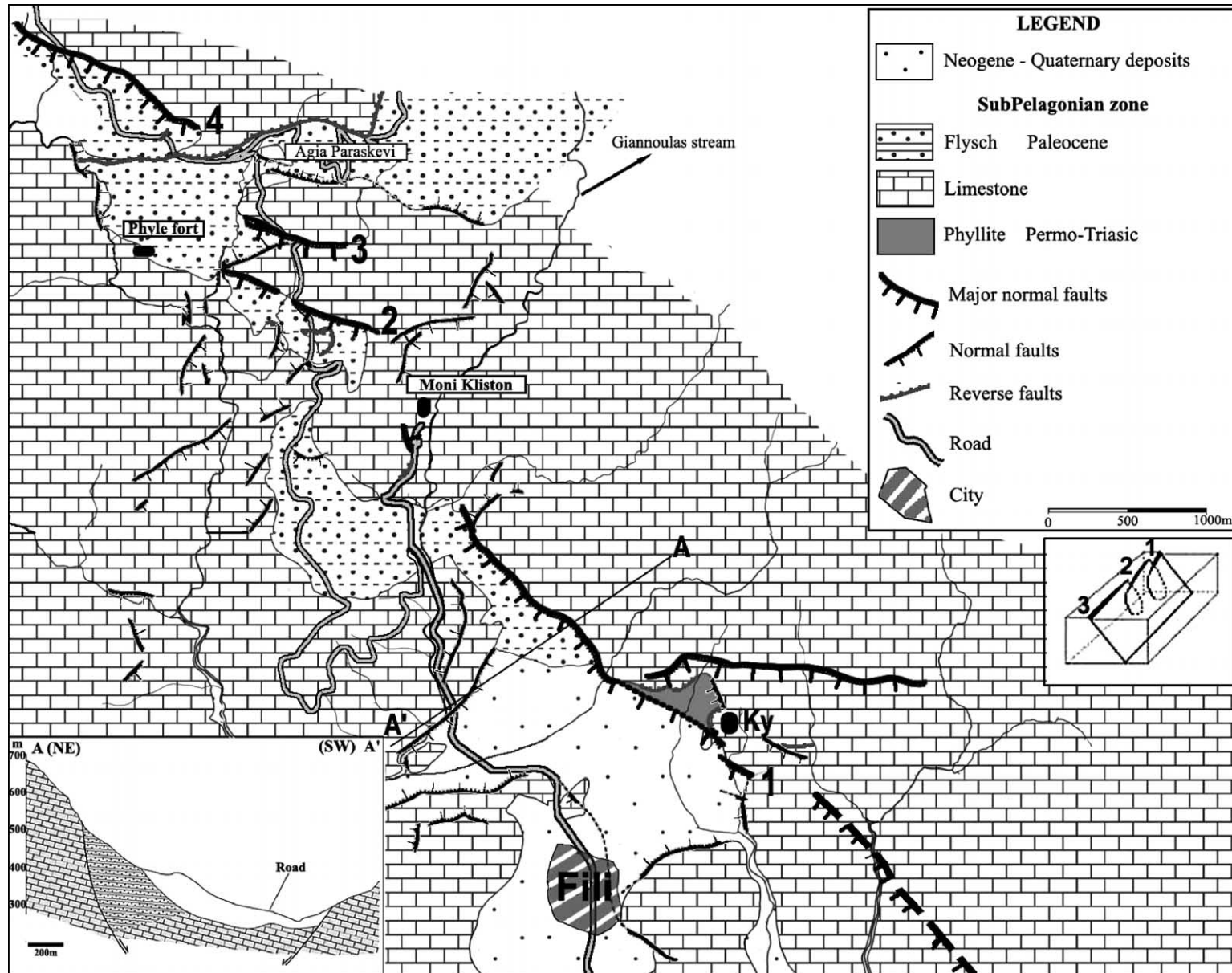


Fig. 2. Geological map of the Fili fault area, Attica, Greece. Arabic numbers indicate fault segments. Box at lower left shows cross-section AA'. Inset cartoon shows segment linkage at depth (after Ferrill et al. (1999); not to scale).

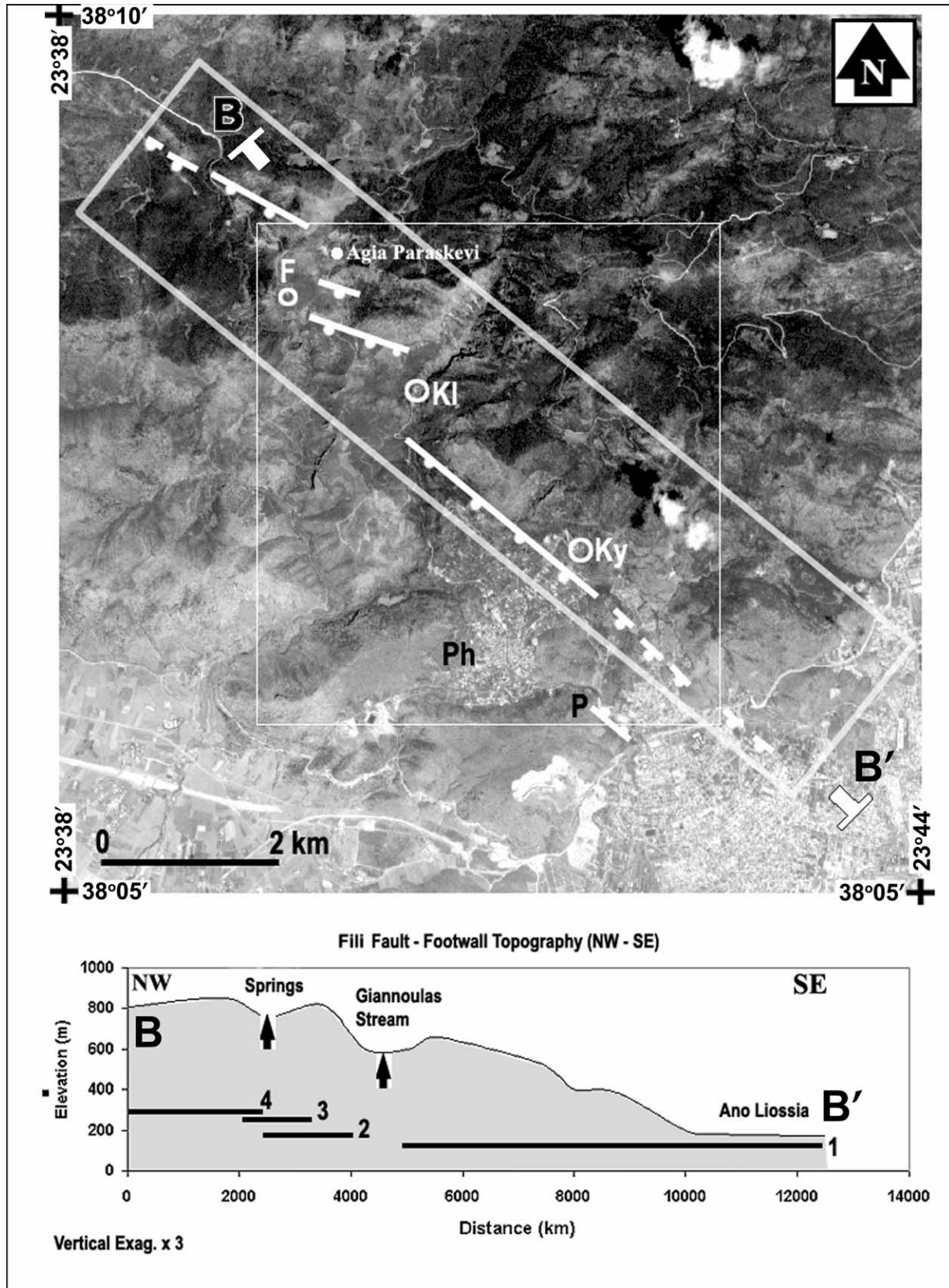


Fig. 3. Greyscale, satellite image of the Fili area, Attica, Greece. Image contrast has been enhanced relative to raw data. Satellite IRS-1C, July 1999. Box indicates extent of Fig. 2. Inclined box shows probable extent of Fili Fault zone and its average strike N125°. Thick white lines indicate normal fault segments (ticks on the hanging wall). Circle Ky shows the locality of Kyprianos Monastery where ground ruptures were observed on September 7th 1999; Circle KI shows the locality of Kleiston Monastery where extensive rockfalls occurred on September 7th 1999 and Circle F indicates the Fili Fort, which was badly damaged during the earthquake. Ph is Fili town and P is Platoma locality where an antithetic ground rupture was observed. Bottom part shows topographic section NW–SE, drawn from B to B'.

planes cannot be detected because they are aligned parallel to the southeastern sun azimuth. However, their position can be inferred by the alignment of long, limestone ridges, which are clearly recognizable by their light grey tone and semi-ellipsoidal shape. In topographic maps, all segments are clearly defined by linear escarpments, across which variable relief exists (20–400 m). It is notable that the northwestern segments occur at higher elevations (Fig. 3, bottom). This may not be coincidental because no synrift was mapped along those segments either. Instead, these segments displace carbonate bedrock against flysch (Fig. 2). The lack of synrift may be associated with a combination of factors such as the small segment length, i.e. small displacement, and erosion.

The main branch of the fault is 4.5 km long (segment 1 in Fig. 2) and defines the small Fili basin of Neogene age that was mapped by Katsikatos et al. (1986). It is probable that this segment continues to the south-east for a distance of about 2 km inside the municipality of Ano Liossia; however, no fault scarps were mapped in that area. This is because (a) a prominent lineament is imaged both in satellite imagery and shaded relief maps (Ganas et al., 2001), (b) towards the SE end of segment 1 a surface break was mapped after the Athens earthquake (letter P in Fig. 3; Pavlides et al., 2002), which was interpreted as gravitational motion along an antithetic fault to segment 1, and (c) geophysical data (Louis et al., 2002) report NW–SE normal fault traces inside the Ano Liossia basin. Although other normal faults also exist with a N40–N50 degrees strike (Fig. 2, north of Ky) they are all cut by the younger, Fili fault.

The second branch (segment) of the Fili Fault lies to the northwest of the main segment at a right-step configuration. This branch is 1200 m long (Fig. 4c). The segment boundary between segments 1 and 2 occurs across a sharp, geomorphological feature, the gorge formed by the Giannoulas stream (see Fig. 3). The third segment has a length of 900 m. This segment exhibits well-developed striations along polished surfaces and fresh basal stripes for about 10% of its length. The height of the stripes ranges between 30 and 50 cm and they are interpreted as a result of footwall uplift/hanging wall subsidence due to seismic motion, although it is not clear if they result from single or multiple normal slip increments. The fourth segment has a length of 1500 m. Fault planes along this segment dip between 50 and 60° (Fig. 4a) and display a narrow basal stripe of about 10 cm on average (Fig. 4b). Within a few tens of metres in the footwall of this segment, near Agia Paraskevi, an area of carstic springs exists (Figs. 2 and 3). According to the Athens Fire Brigade people who occupied an observation post nearby, the water of the springs disappeared for about 3 h before the 7/9/1999 earthquake. Also, in the hanging wall of segment 4, and in the northwestern prolongation of segment 3, is the Fili Fort (letter F in Fig. 3; Fig. 4c; known as Phyle Fort in

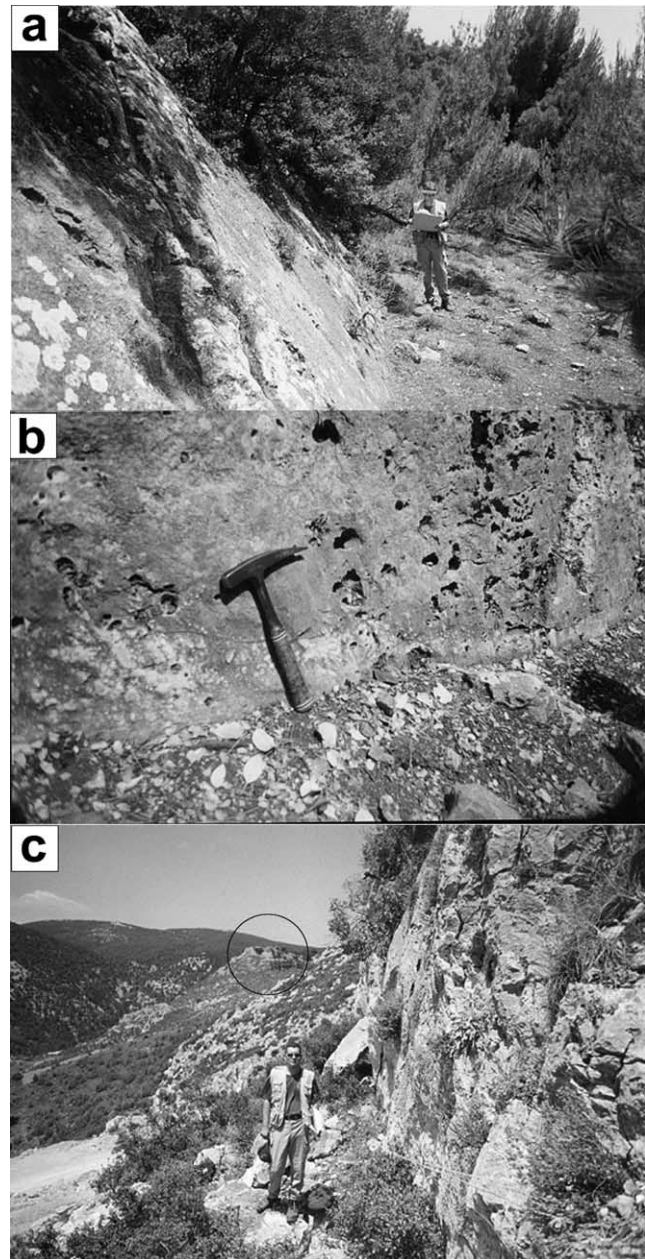


Fig. 4. (a) Field photograph of the fault plane along the fourth branch (segment) of the Fili fault. View to the east. (b) Close-up of locality shown in (a) with fresh slip surfaces shown at the base of the scarp. (c) Field photograph of the normal fault plane comprising the second branch (segment) of the Fili Fault. The geologist stands on the hanging wall. The ancient fort of Fili can be seen in the background (black circle). View to the northwest.

archaeology), which was seriously damaged during the 7/9/1999 earthquake (Papadopoulos et al., 2002).

Note that the terminations of the distal fault segments (1 and 4) are poorly exposed because no fault-generated topography exists (e.g. King et al., 1988). We infer probable terminations for both segments as fault throw approaches zero. Therefore, we estimate an error of 5% (missing lengths at fault tips) although larger errors are also probable. This brings the estimated fault length to 8.5 km. Average spacing

between segments is 700 m with no overlap except for segments 2 and 3, where overlap is almost 50%.

The stratigraphic offset of the pre-rift across the fault is difficult to establish, because of the absence both of the flysch–limestone contact in the footwall (which exists in the hanging wall; section AA' in Fig. 2) and of the phyllite–limestone contact in the hanging wall. However, a minimum throw estimation is available because at least 320 m (top of Cretaceous limestone) offset of the pre-rift is exposed to the north of the Fili town (Fig. 2). In addition, the Neogene (4 Ma) basin fill amounts to 300 m (Katsikatsos et al., 1986). Assuming a pre-rift flat topography we derive an offset of about 620 m or a cumulative, dip-slip displacement of 715 m for segment 1 (assuming a dip-angle of 60° to the SW; see Fig. 12 below). It follows that the mean slip rate is 0.18 mm/yr.

### 3.2. The Avlon and Maliza Faults

#### 3.2.1. Avlon Fault

The northern side of Parnitha is bounded by the Avlon Fault (Letter A in Fig. 1a; Papanikolaou et al., 1988; Galanakis et al., 1997; Goldsworthy et al., 2002). The fault has a clear geomorphic expression with limestone ridges aligned along its footwall (Fig. 5, top). The elevation data (HAGS, 1978) across the fault show two distinct parts, a flat area to the north (hanging wall) and an elevated, bedrock area to the south (footwall), with elevations in the latter reaching 933 m (HAGS, 1978; Fig. 5). The footwall elevations decrease systematically towards the fault tips (see arrow in Fig. 5, top). The hanging wall areas range between 150 and 200 m above sea level. Taking into consideration the estimated syn-rift thickness in the vicinity of Avlon (Tanagra–Malakasa basin of Mettos et al. (2000)), which exceeds 600 m, we may accept a 600 m basin fill near the town of Avlon (letter A in Fig. 5). Therefore, a minimum throw estimate across the Avlon fault reaches 1500 metres and by trigonometry we derive a total offset across this fault of about 2000 m, assuming fault dip of 50° and flat pre-rift topography. This slip can be divided by the oldest age estimate for the syn-rift, which is of Upper Miocene age, because of drilling into Upper Miocene (Vallesian; 10 Ma) beds near Avlon (Mettos et al., 2000). This age constraint yields an estimate for the mean slip rate of about 0.2 mm/yr.

#### 3.2.2. Maliza Fault

In the region of Oropos (north of A in Fig. 1a; Fig. 5 bottom), which is situated to the north of the Avlon fault, several normal faults have been recognised previously (Papanikolaou et al., 1988; Goldsworthy et al., 2002). However, our field mapping shows that in the hanging wall of the Avlon Fault a 2–5-m-high, 4.7-km-long, limestone scarp runs along the base of the Maliza hill (M in Fig. 5), immediately to the south of the national motorway (Fig. 6). The base of the scarp comprises a continuous slip surface, bearing normal-slip striations (Fig. 7). The Maliza footwall

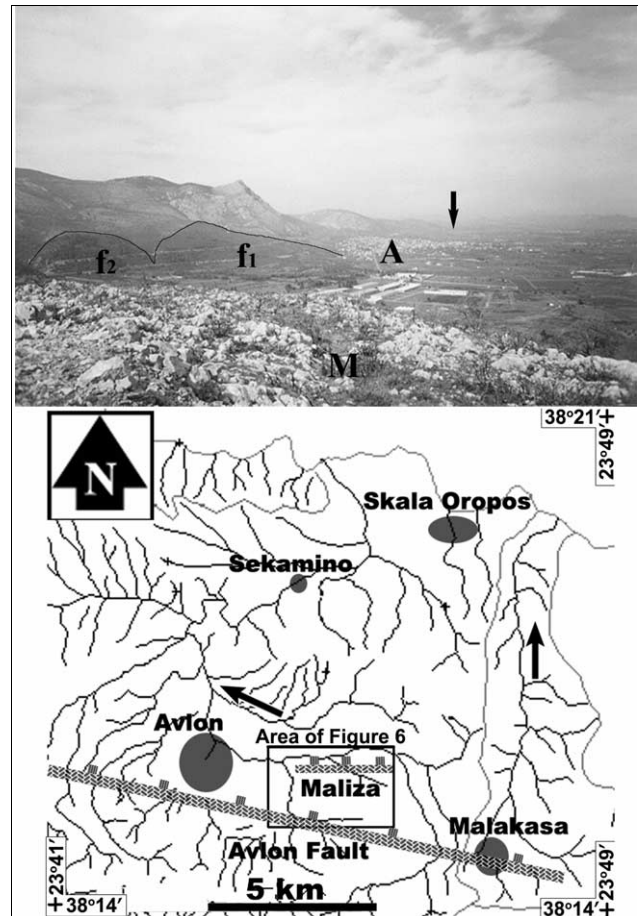


Fig. 5. (Top) Field photograph of the Avlon Fault segment, March 2001.  $f_1$  and  $f_2$  indicate degraded triangular facets developed on carbonate bedrock. Facet edges are indicated by thin black lines. Vertical black arrow points to fault tip area. The town of Avlon is indicated by the letter A. View to the west from the Maliza hill (M). (Bottom) Drainage map of the Avlon region showing different stream directions (black arrows) along strike of the Avlon Fault (shaded rectangle with ticks on the downthrown side). Dark grey lines show stream courses and light grey lines indicate the extent of catchments. Inset box shows extent of Fig. 6.

pre-rift (Fig. 6) is composed of thick, Cretaceous limestones and small occurrences of Upper Palaeozoic schists. The syn-rift comprises terrestrial Neogene deposits, mainly lacustrine marls, clays, and fluvial conglomerates. Quaternary deposits cover unconformably the Neogene strata as well as the pre-rift rocks. Around Avlon these deposits are dominantly fluvial and attain large thickness (Mettos et al., 2000). The sediments include incohesive conglomerates, clays, clay silts, and sands in intercalations and appear brown–red in colour. Immediately to the west of Maliza hill along a natural section we observed stream deposits of probable Upper Pleistocene–Holocene age dipping to the south between 10 and 15°.

The Maliza fault was mapped at 1:5000 scale and we collected fault-slip data from 26 localities. We also note that the height of the scarp ranges from 5 m in the middle to 1 m at both ends and this reduction is systematic towards fault tips. Furthermore, this height profile matches the elevation

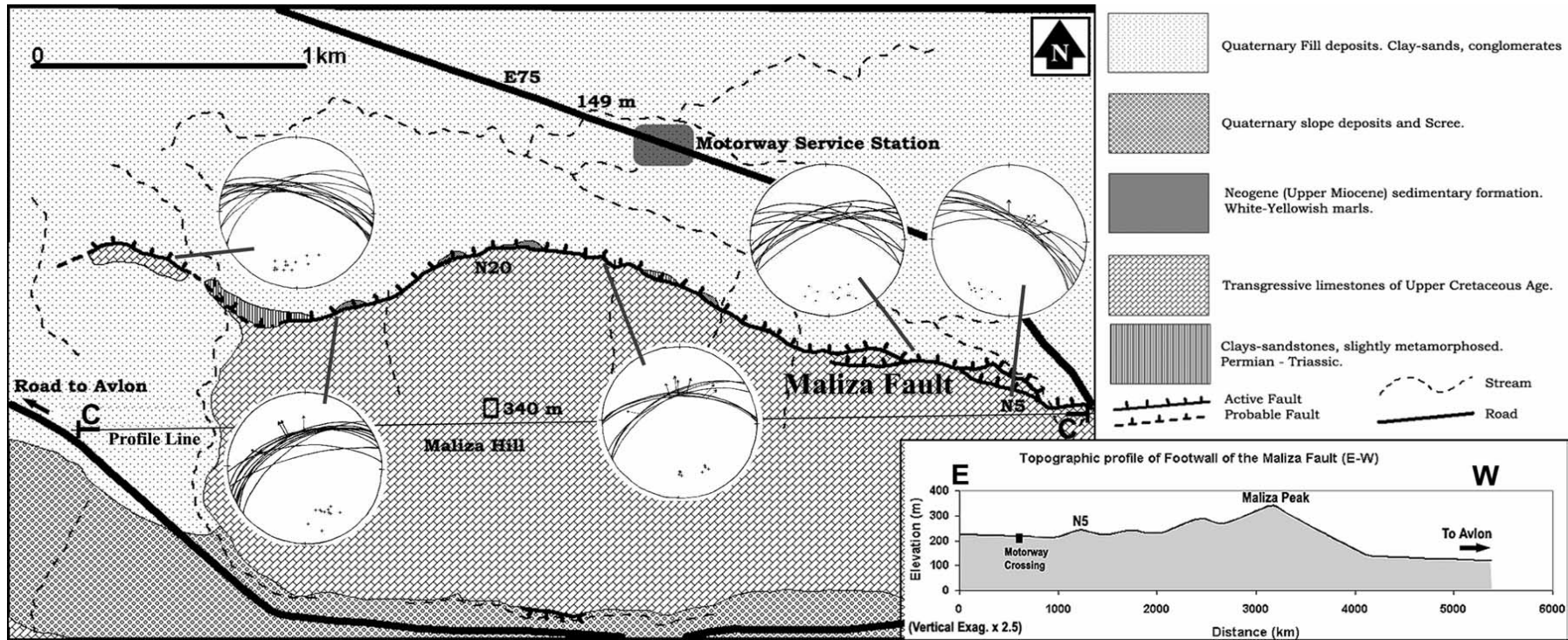


Fig. 6. Neotectonic map of Maliza area. Thick line with ticks identifies the Maliza Fault. Stereographic projections indicate fault plane orientation and slip direction at selected localities along strike. Inset shows an E–W elevation profile of the footwall along the line C–C'.

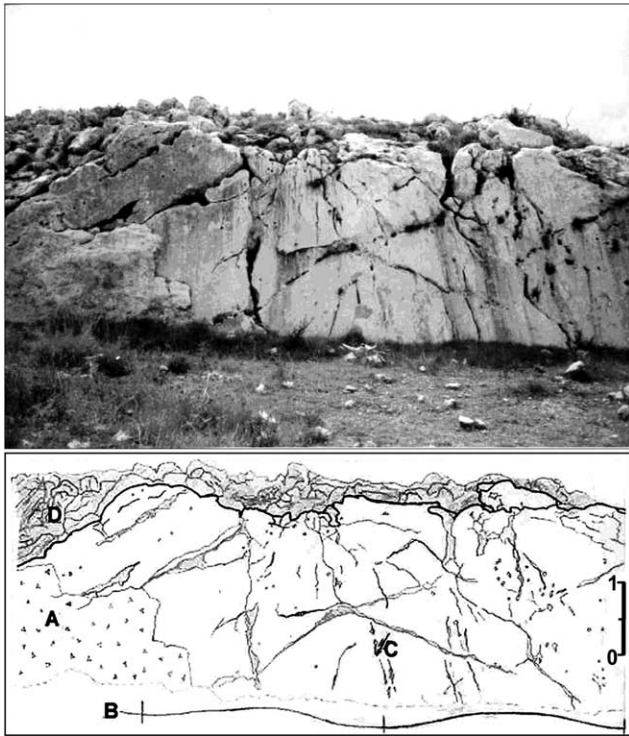


Fig. 7. (Top) Field photograph of the Maliza fault scarp (March 2001). Height of scarp is about 4 m. This is locality N5 on the map shown in Fig. 6. View to the south. (Bottom) Line drawing of top figure. A indicates fault gouge, B indicates scarp curvature (3.6 m) and C points to the trend of the slip vector. Thick grey line near D indicates limit of increased erosion due to rainfall.

profile of the footwall, the Maliza hill (Fig. 6, line C–C'), which shows an elliptical geometry similar to other normal faulting localities in central Greece (e.g. Roberts and Ganas, 2000). Most of the scarp runs parallel to the 180–200 m elevation contours along the E–W direction. At several localities the fault scarp is corrugated at wavelengths ranging from 3–4 m to a few tens of metres (localities N5 and N20 in Figs. 6 and 7). Corrugated fault planes are a characteristic feature of normal faults (e.g. Ganas et al., 1998; Ferrill et al., 1999; Roberts and Ganas, 2000) and their formation is related to fault growth processes.

In terms of scarp morphology, the scarp surface is covered locally by a thin, white crust of calcitic powder, which is interpreted to result from chemical weathering of the scarp's surface (Fig. 7). In many localities we observed noticeable differences in the surface roughness of the scarp, usually a smoothing gradient towards the base of the scarp. We were able to distinguish at least one stripe of light, grey surface at the base of the scarp (Fig. 6, locality N20), and approximately 30 cm thick. This smooth part of the scarp most probably indicates the latest reactivation of the Maliza fault plane.

To summarise, the Maliza scarp height varies along strike and shows values ranging from 1 to 5 m, bears fresh basal stripes and slickenlines. We suggest that the scarp was

formed by repeated co-seismic uplift along an active fault that defines the now-active boundary of the Plio-Pleistocene basin. As such this fault has hosted several earthquake ruptures during Late Quaternary times. We also suggest that the Maliza Fault can host large earthquakes ( $M_w \geq 5.8$ ) as it may continue to the west of the Maliza hill (Fig. 5) towards the city of Avlon. It is reasonable to assume that the Maliza Fault may be linked to the Avlon Fault to the west (towards the town of Avlon) because we mapped tilted alluvial beds to the west of the Maliza Hill. On the contrary, the Maliza Fault does not continue further to the east (i.e. towards the area of Malakasa) because the hanging wall drainage flows to the north (see black arrows in Fig. 5). Furthermore, by using footwall topography as a proxy for fault throw (e.g. Roberts and Ganas, 2000) and based on the small throws observed along the Maliza Fault (Fig. 6) it is probable that the fault slip rate during this period does not differ significantly from the older Avlon Fault. A more precise estimate is not possible because the net thickness of sediments is unknown.

### 3.3. The Thrakomakedones Fault

The southern boundary of Parnitha is a linear mountain front with large alluvial fans spreading outwards. Several large escarpments exist in the general NE–SW orientation. We focused our attention in the area of Thrakomakedones that was strongly hit by the September 7th 1999, event (Papadopoulos et al., 2000; Pomonis, 2002; letter T in Fig. 1a). A satellite image in Fig. 8 (5.8 m spatial resolution; see area marked by letters TH) taken in July 1999 (before the Athens earthquake) shows a corridor of urban development from south to north, crossing a probable fault line.

Our geological field mapping in Fig. 9 showed two neotectonic, possibly active, faults, both with normal-slip geometry and similar strike (N60), and downthrowing to the south-southeast. One fault is indicated by a 4-km-long, continuous scarp, running along the base of the Parnitha foothills. Several well-defined slip surfaces exist along the eastern portion of the fault (e.g. Fig. 10). It is not clear why the typical fault architecture (e.g. Hancock and Barka, 1987; Stewart and Hancock, 1988, 1991) appears only at the eastern part. This is worthy of further investigation because the Thrakomakedones Fault defines the boundary of the Neogene basin (Fig. 9) and it should exhibit similar fault zone architecture along its strike. This locality (N6) exposes a 4 m high scarp. The architecture of the fault zone is defined by a series of breccia 'layers', described below from the fault plane outwards. It starts with the polished surface (1) of the fine-grained, brecciated limestone, continues to hanging wall, limestone coarse-grained breccia (2), to a narrow sheet consisting of small limestone pebbles in a red matrix (3), goes on again to a coarse-grained limestone breccia (4) and ends with the development of a rather weak slip surface (5) with calcite powder. It is suggested that this

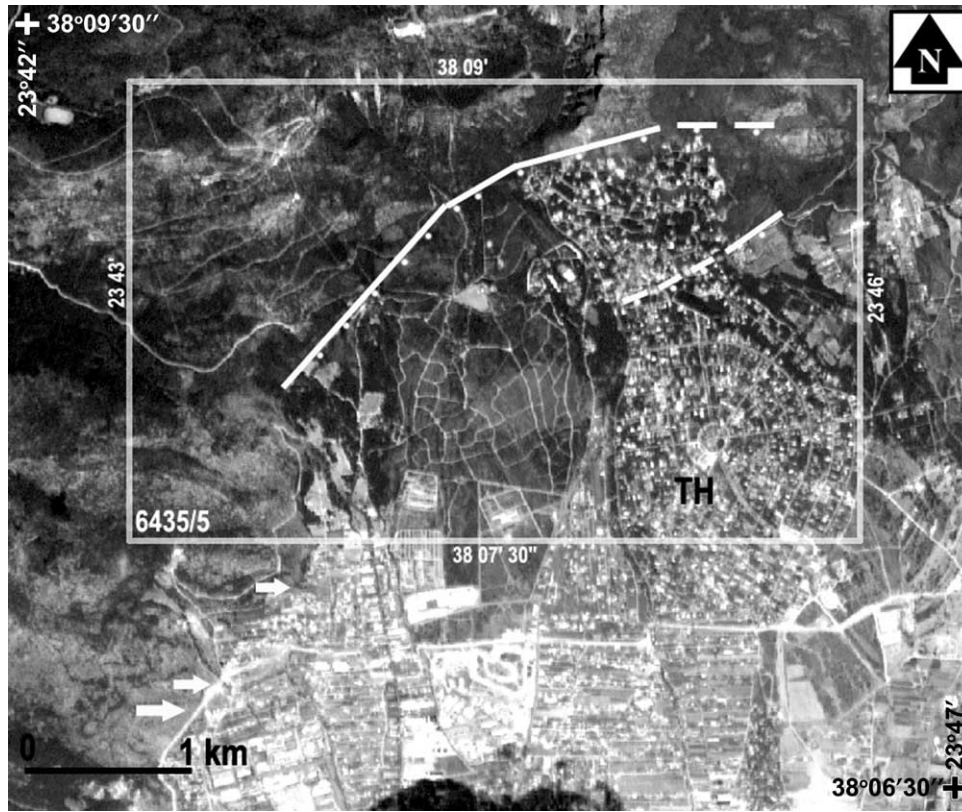


Fig. 8. Greyscale, satellite image of the Thrakomakedones area, Attica, Greece. White box shows extent of Fig. 9. Continuous white line indicates position of normal fault scarp. Dashed white line indicates fault prolongation. White arrows point to possible southwestern continuation of normal fault. Image contrast has been enhanced relative to raw data. Satellite IRS-1C, July 1999.

zoned architecture reflects periods of faster versus slower slip rates during a fault's life. Faster slip rates result in the formation of the coarse-grained breccia sheets, composed of angular limestone fragments, whereas less active periods result in the formation of incohesive breccia in red clay matrix. Finally the fault zone is partially covered by Quaternary colluvium. The western part of the fault is not clear in the satellite imagery (Fig. 8) because of the small height of the scarp and the dense vegetation.

The second fault is located in the hanging wall area of the former, has a sub-parallel strike and similar dip direction (to the southeast). The height difference between the two faults is 140 m. This fault is discontinuous and outcrops in the adjacent area of the Panagia Monastery (Fig. 9). Its western prolongation is assumed to lie beneath the alluvial fan of the Thrakomakedones area. An indirect evidence for this is the sharp deflection of the Agia Triada stream about 800 m to the south of the Thrakomakedones Fault (see inset box in Fig. 9). We also note that there is another small segment further to the southwest (see horizontal white arrows on the satellite image; Fig. 8). This segment is located right on the sharp mountain front. This front may also indicate the activity of a normal fault, possibly linked to the Thrakomakedones Fault.

We tried to quantify the slip rate along the Thrakoma-

kedones Fault by looking for suitable stratigraphic markers. Our mapping showed uplifted, synrift beds (marls) at a height of about 580 m near locality N29 (Fig. 9). These lacustrine rocks may correspond to the Turrolian beds (5 Ma; Mettos et al., 2000), which may comprise the oldest beds of the NW Athens basin. The Neogene thickness in the greater Thrakomakedones area does not exceed 500 m (Freyberg, 1951). If this is so we may correlate the base of the synrift on either side of the fault and estimate a vertical offset (throw) of about 1080 m or a down-dip cumulative slip of 1240–1300 m (for a fault dip between 55 and 60°). In turn, this yields a mean slip rate of about  $0.25 \pm 0.01$  mm/yr for the Thrakomakedones Fault. However, there are two uncertainties: (a) it is possible that the 1080 m throw was accumulated by motion along two parallel, active faults as indicated in Fig. 9 and (b) it is possible that the age of rifting is older (Upper Miocene) as in the Avlon basin.

#### 4. Kinematic analysis–interpretation

We present a synthesis of 63 measurements of the orientations of fault-planes, frictional-wear striae on fault planes, and corrugations of fault planes from tens of study sites around Parnitha (Fig. 12). Displacements on

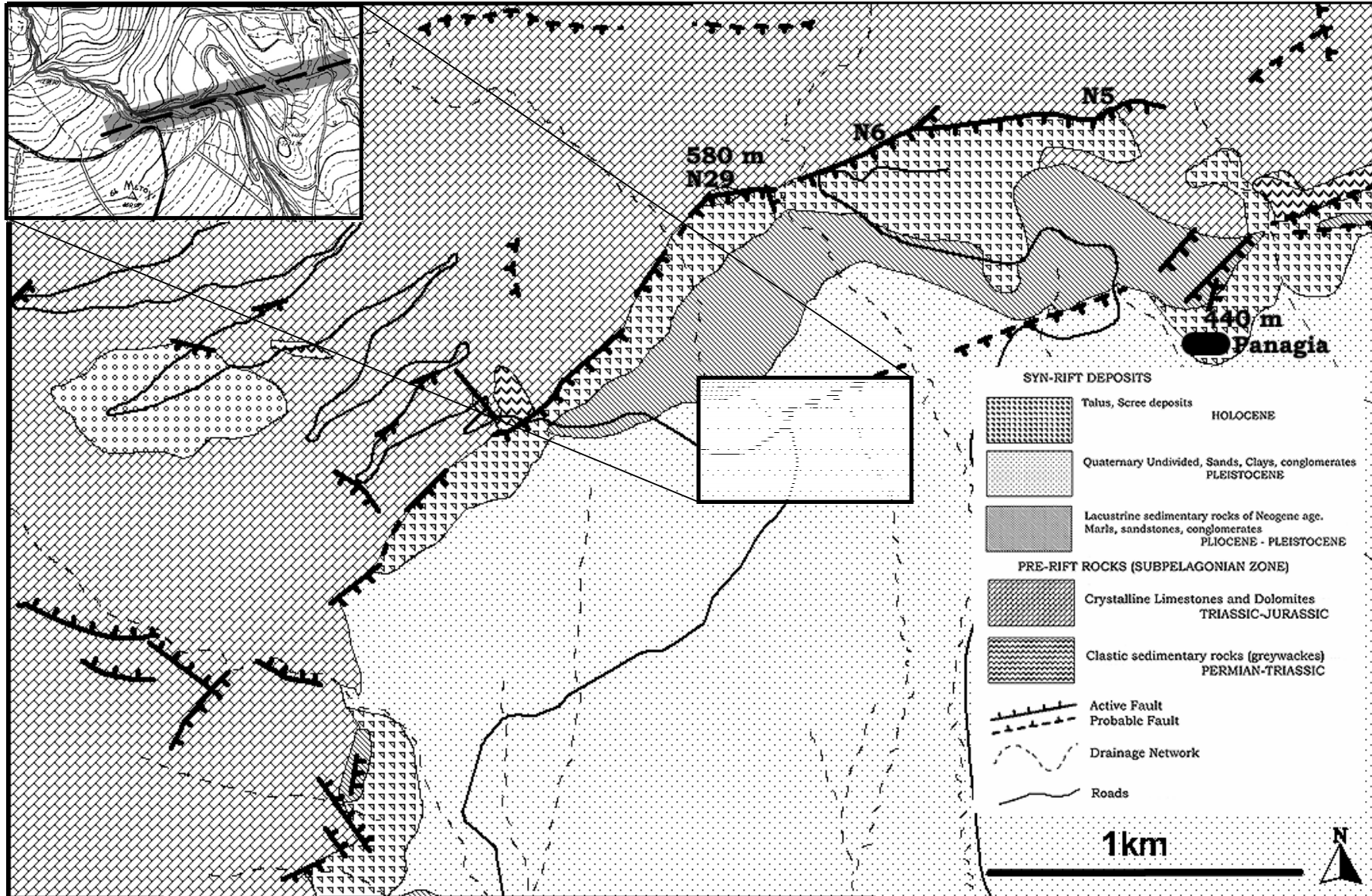


Fig. 9. Neotectonic map of Thrakomakedones area. Thick line with ticks identifies the Thrakomakedones Fault. Upper left box is a portion of the 1:5000 topographic map showing stream deflection across a possible normal fault. The map background (roads, streams) is from the 1:5000 map sheet 6435/5 of the Hellenic Army Geographical Service.

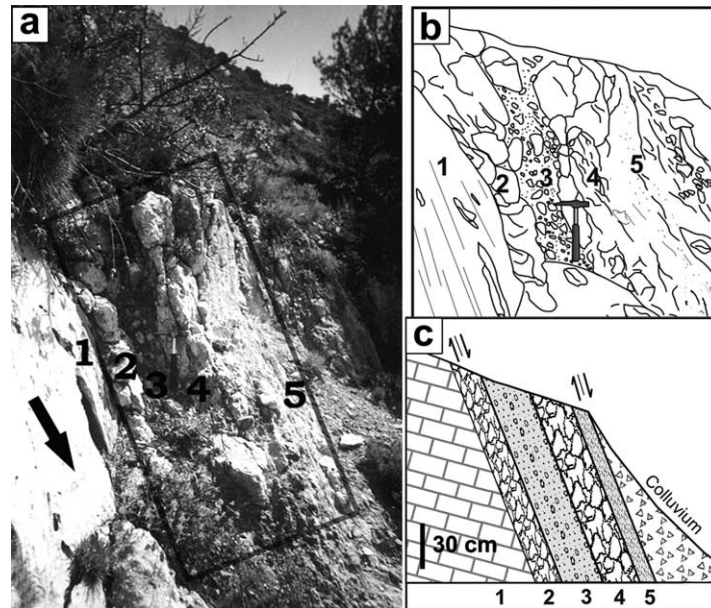


Fig. 10. (a) Field photograph of locality N6 along the Thrakomakedones Fault (see Fig. 9 for location) showing a section of the fault architecture. Black arrow indicates sense of motion along the slip surface. Inclined box indicates size of cataclastic zone with thickness 0.9 m. Note hammer for scale. View to the northeast (July 2002). (b) Outline of the fault architecture showing five different layers of fault breccia. (c) Model cross-section of fault zone development. The fault juxtaposes Mesozoic limestone (in the footwall) with Quaternary colluvium (in the hanging wall). The fault zone is characterised by alternating incohesive breccia belts (three and five) and compact breccia sheets (two and four). The alternating breccia structure may result from the variation in fault slip rate during a fault's life.

the faults ranged from a few metres (Maliza) to several hundred metres (Fili) and as much as 1200 m (Thrakomakedones). We measured the strike and dip of the fault plane associated with each striation and corrugation. We measured both the strike and dip of such fault surfaces with a hand-held, CLAR type compass to within  $5^\circ$  total error. Then we measured the rake and the slip-direction of the striations and corrugations, again using the same hand-held compass. Again, we measured the rake to within about  $5^\circ$  total error.

We analysed all fault slip data for stress axes orientation by the FAULT software for Windows (Caputo and Caputo, 1988). We included all measurements for the Fili Fault (Fig. 2) and the Maliza Fault (Fig. 6) despite the fact that slip surfaces showed a wide variety of orientations. This happened because all slip surfaces showed evidence for recent activity such as (a) a polished slip plane and (b) a light grey stripe along the base of scarp. Both faults bear striations with high rakes (Fig. 12). Pavlides et al. (2002) also report near-vertical fault slip data from segment 1 collected at localities near the Kyprianos Monastery (Ky in Fig. 3; see Figs. 7 and 8 of Pavlides et al., 2002). We did not process the data for the Thrakomakedones Fault because we mapped a systematic difference in fault scarp morphology from NE to SW, implying a different seismic history along strike. The fault plane orientation data are presented in Fig. 11, in both equal-area stereographic projection form and as rose diagram. A

dominant NE–SW strike is seen despite the scatter in the pole density data (Fig. 11b).

Two methods were applied: the *right dihedral* (Angelier and Mechler, 1977; middle set of stereonets in Fig. 12) and the *conditional square minima* (Caputo and Caputo, 1988; white set of symbols in Fig. 12). Both methods assume that fault motion occurs along the maximum resolved shear stress direction. Both methods produce a tensional field as indicated by the plunge and azimuth of the least compressive stress  $\sigma_3$  axis. The  $\sigma_3$  axis is sub-horizontal and has a general orientation NNE–SSW ( $N196^\circ$ – $N206^\circ$  for Fili;  $N7^\circ$ – $N12^\circ$  for Maliza).

Although we did not measure co-seismic surface slip we note that this stress field is compatible with the trend of the T-axis of the Athens earthquake focal plane solution (HRV  $N19^\circ$ , USGS  $N221^\circ$ ; Fig. 1b). This coincidence of fault slip directions and T-axes azimuth was also demonstrated for the eastern Gulf of Corinth area, on the basis of the 1981 aftershock distribution (Morewood and Roberts, 2001). Such observations show the continuity in time of the stress field near active faults, i.e. stress analyses of Late Quaternary fault-slip data agree with present-day, coseismic stress pattern as mapped by the T-axes azimuth of the mainshock. In addition, the  $\sigma_3$  trend in Parnitha agrees with the extension direction found by Roberts and Ganas (2000) inside the Gulf of Evia rift ( $N14^\circ$ ) and not with the one in the Gulf of Corinth ( $N353^\circ$ ). This important point is discussed below.

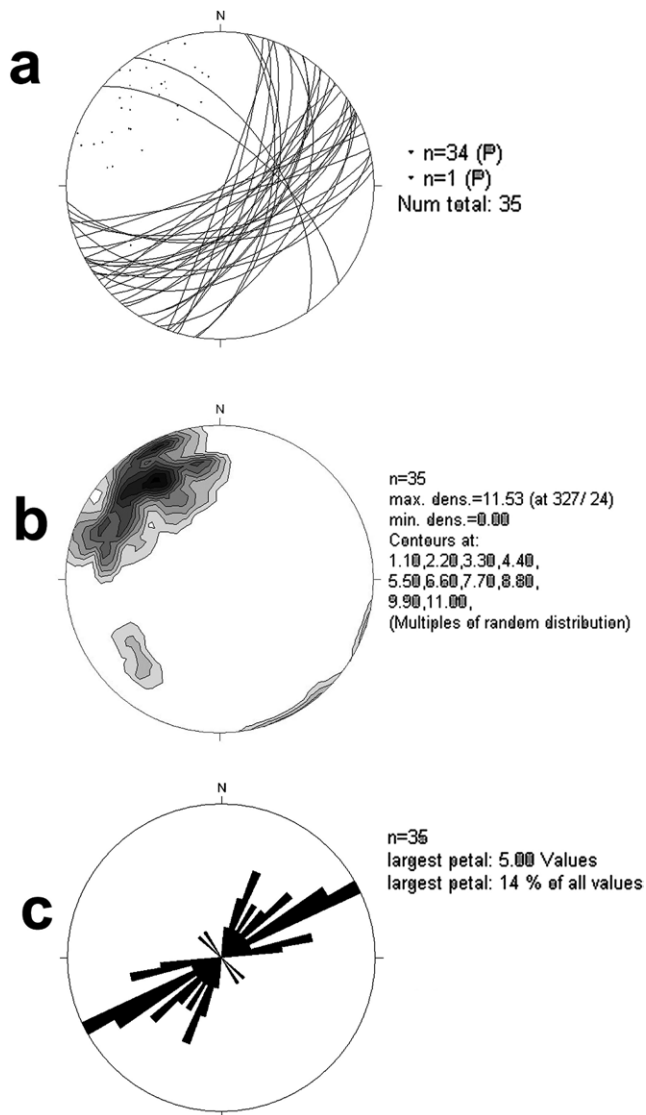


Fig. 11. Synthesis of kinematic data from the Thrakomakedones Fault. (a) Stereographic projections of fault planes ( $N = 35$ ), (b) projections of poles to fault planes, and (c) rose diagram of strikes of fault planes in  $10^\circ$  intervals. The dominant NE–SW orientation is clearly seen.

## 5. Discussion and summary

### 5.1. Segment geometry, lengths and segmentation pattern

The three mapped faults in Parnitha show lengths between 4 and 8.5 km. Two of the faults (Maliza, Thrakomakedones) comprise one segment, while the Fili Fault (Fig. 3) comprises four segments. We note that no overlap zone larger than 1 km occurs along the Fili Fault, indicating that the individual segment boundaries may not inhibit or halt a propagating rupture along the fault (e.g. Crone and Haller, 1991). Moreover, it is possible that the four right-stepping, en-échelon segments merge into a single planar fault plane at seismogenic depths (8–12 km; see inset model in Fig. 2). We also note that the Fili Fault

throw decreases from the end of segment 1 and to the northwest; however, absolute elevations increase (Fig. 3). This may indicate late linkage of the three northern segments to segment 1 (Fig. 2). Of further interest is where the Parnitha faults are linked to other faults along strike or not. Our study could not confirm this hypothesis for the Fili or Thrakomakedones Faults; however, for the Maliza fault this cannot be rejected.

The Maliza Fault is a young, normal fault formed in hard Mesozoic limestone. The fault has a total length of 4700 m and strikes E–W. It is probable that the Maliza hill was an intrabasin high in the footwall of the older, Avlon Fault, separating the Malakasa basin to the east (Galanakis et al., 1997) from the Avlon basin to the west. This hypothesis gains support from two pieces of evidence. Firstly, axial drainage has developed in the hanging wall of the Maliza Fault with a western flow direction (Figs. 5 and 6) while in the neighbouring Malakasa basin drainage flow is to the north (Fig. 5; Papanikolaou et al., 1988; Galanakis et al., 1997). Secondly our mapping shows that the Maliza Fault has a convex geometry in map view (Fig. 6), which seems to follow the pre-rift morphology of the ridge. This rupture is consistent with the hanging wall migration model of fault activity within rift systems (Stewart and Hancock, 1991; Goldsworthy and Jackson, 2000, 2001), in this case away from the older, Avlon Fault approximately 2 km south of Maliza. The Avlon Fault, by contrast, does not form a continuous scarp and there is no evidence for recent activity (such as acute triangular facets, slip surfaces etc.) in the zone south of the Maliza Fault. Consequently, although we cannot rule out the possibility that the Avlon Fault is active today throughout its length, we conclude that the Maliza Fault poses the main seismic hazard threat to Avlon and surroundings.

Of interest to rupture history studies along the Maliza Fault is the combination of the fault's single segment geometry with scarp curvature. First, the existence of fresh basal stripes indicates recent (Holocene) seismic motion as in other faults in Greece (Stewart and Hancock, 1991; Ganas et al., 1998) and elsewhere (Pavlidis et al., 1999; Michetti et al., 2000). Second, assuming that former earthquakes ruptured the entire of the Maliza fault plane, we observe two localities along strike where the fault plane splits upwards in two branches (Fig. 6). In both cases the upslope branch joins to the main fault plane creating a 'rhomb' slice of footwall for about 400 m in the long dimension (see locality N5 in Fig. 6). At the easternmost locality the fault strike changes  $70^\circ$ , with a  $40^\circ$  change in the more central one. Thus, the curved geometry of the Maliza Fault plane did not prevent repeated earthquakes to rupture without disrupting the single segment geometry.

### 5.2. Slip rates and earthquake occurrence

Although we calculated mean slip rates from single-point observations across the Fili and Maliza faults, fault-scarp

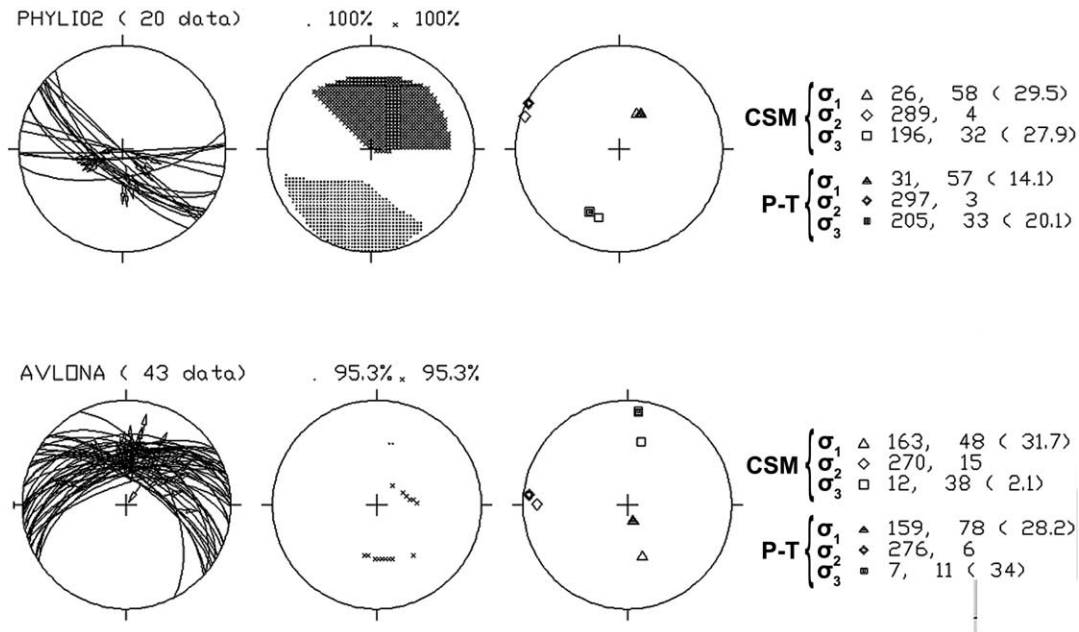


Fig. 12. Quantitative stress analysis along the Fili Fault (top) and Maliza Fault (bottom). Left: striated slip surfaces are presented in lower hemisphere, equal-area stereographic projection as major circles. Slip directions are shown with black arrows. Middle: application of right dihedron method (Angelier and Mechler, 1977) where black is the area of 100% containing  $\sigma_1$  (or P) axis and light colour areas (dots) containing the  $\sigma_3$  (or T) axis. Notice the 95.3% probability for this dataset due to the highest curvature of the Avlon fault plane. Right: determination of the principal stress axes by the method of Caputo and Caputo (1988), major axis of  $\sigma_1$  (triangles) intermediate axis  $\sigma_2$  (circles) and minor axis  $\sigma_3$  (squares). P–T axes are in black symbols, CSM axis are in white symbols, respectively.

morphology does not vary significantly along strike of faults (as would be expected if there were different ages in scarp formation). Where there is along-strike variation of slip rates, then faster footwall uplift rates would produce ‘sharper’, smoother surfaces along strike, in contrast to slow-moving parts of the fault. However, along the Thrakomakedones Fault, scarps exhibiting smooth, polished surfaces do appear at several localities (Fig. 10) but mainly on its eastern part. At locality N29, approximately 500 m to the west of Fig. 10, the fault plane is visible but weathered. In contrast, both Maliza and Fili Faults exhibit a relatively uniform bedrock scarp morphology, similar to the one described by Hancock and Barka (1987).

A relative assessment of Late Quaternary fault activity can be made on the basis of both geological and seismological data. First, the length of the Fili Fault is considerably longer than the Maliza and Thrakomakedones Faults, implying a more efficient strain localisation. Second, the Thrakomakedones fault resides in the greater, footwall area of the Fili Fault, because (a) to the southwest of Thrakomakedones Fault the topography is controlled by the NW–SE Fili Fault (Fig. 1a and b) and (b) the central Parnitha drainage belongs to the catchment of the Giannoulas stream, which develops in the footwall of the Fili Fault (Fig. 3). Third, the E–W Maliza Fault is a Late Quaternary structure because of scarp freshness and small height (Fig. 7). Fourth, the Athens Mw5.9 earthquake most probably

occurred along the Fili Fault (Pavlidis et al., 2002; Sargeant et al., 2002). Therefore, we suggest that the NW–SE structures localize present-day strain more efficiently.

Our results show that the *mean* slip rates of the three active faults in Parnitha (0.18–0.25 mm/yr) are comparable with slip rates along active normal faults inside the Gulf of Evia graben (e.g. Ganas et al., 1998; Pantosti et al., 2001; 0.27–0.4 mm/yr). In comparison they are much lower (an order of magnitude less) than slip rates derived from trrenched-faults inside the Gulf of Corinth rift (e.g. Collier et al., 1998, 1–3.5 mm/yr; Koukouvelas et al., 2001; 1.5 mm/yr). This important difference may be due to higher seismic strains inside the Gulf of Corinth. This has been confirmed by GPS measurements of crustal extension in central Greece (e.g. Clarke et al., 1998) and seismic moment release comparisons for the last 240 years (Papazachos et al., 1991). Therefore, it appears that the Gulf of Corinth remains an ‘isolated’ area of high crustal extension within the central Greece extensional province.

Although we have no field evidence it is reasonable to extend this low slip-rate data obtained for the Parnitha faults to other fault segments around Athens, based on historic seismicity records (see review in Papadopoulos et al. (2002)). Such ‘slow’ active faults may be responsible for the large recurrence intervals of destructive earthquakes near Athens.

## Acknowledgements

This research was funded by the Earthquake Planning and Protection Organisation of Greece (OASP), the General Secretariat for Research and Technology of Greece and the National Observatory of Athens. We thank George Stavrakakis, Yannis Koukouvelas, Gerald Roberts, Leonidas Stamatopoulos, Dimitris Galanakis, Stella Kortekaas, Hiro Matsumoto and Vassilis Karastathis, for discussions. We also thank Nigel Morewood and Iain Stewart for constructive reviews and D.A. Ferrill for editorial assistance. Fig. 1b was prepared with GMT. The IRS satellite image was provided by ZOElectronic.

## References

- Ambraseys, N.N., Jackson, J.A., 1990. Seismicity and associated strain of central Greece between 1890 and 1988. *Geophysical Journal International* 101, 663–708.
- Angelier, J., Mechler, P., 1977. Sur une méthode graphique de recherché des contraintes principales également utilisable en tectonique et en séismologie: la méthode des dièdres droits. *Bulletin de la Société Géologique France* 19, 1309–1318.
- Caputo, M., Caputo, R., 1988. Structural analysis: new analytical approach and applications. *Annales Tectonicae* 2, 84–89.
- Clarke, P.J., Davies, R.R., England, P.C., Parsons, B., Billiris, H., Paradissis, D., Veis, G., Cross, P.A., Denys, P.H., Ashkenazi, V., Bingley, R., Kahle, H.G., Muller, M.V., Briole, P., 1998. Crustal strain in central Greece from repeated GPS measurements in the interval 1989–1997. *Geophysical Journal International* 135, 195–214.
- Collier, R.E.L., Pantosti, D., D’Addezio, G., De Martini, P.M., Masana, E., Sakellariou, D., 1998. Paleoseismicity of the 1981 Corinth earthquake fault: seismic contribution to extensional strain in central Greece and implications for seismic hazard. *Journal of Geophysical Research* 103(B12), 30001–30019.
- Crone, A.J., Haller, K.M., 1991. Segmentation and the co-seismic behaviour of Basin and Range normal faults: examples from east-central Idaho and southwestern Montana, USA. *Journal of Structural Geology* 13, 151–164.
- Ferrill, D.A., Stamatakos, J.R., Sims, D., 1999. Normal fault corrugation: implications for growth and seismicity of active normal faults. *Journal of Structural Geology* 21, 1027–1038.
- Freyberg, von, B., 1951. Das Neogen gebiet nordwestlich Athen, Publication of Subsurface Research Department, Ministry of Coordination.
- Galanakis, D., Mettos, A., Mataragas, D., Triantafyllis, M., 1997. Landslide of Malakasa area, geological and tectonic regime. In: Marinos, Koukis, Tsiambaos, Stournaras (Eds.), *Engineering Geology and the Environment*, Balkema, Rotterdam, pp. 665–670.
- Ganas, A., Roberts, G.P., Memou, T., 1998. Segment boundaries, the 1894 ruptures and strain patterns along the Atalanti Fault, central Greece. *Journal of Geodynamics* 26, 461–486.
- Ganas, A., Papadopoulos, G., Pavlides, S.B., 2001. The 7th September 1999 Athens 5.9 Ms earthquake: remote sensing and digital elevation model inputs towards identifying the seismic fault. *International Journal of Remote Sensing* 22, 191–196.
- Goldsworthy, M., Jackson, J., 2000. Active normal fault evolution in Greece revealed by geomorphology and drainage patterns. *Journal of the Geological Society London* 157, 967–981.
- Goldsworthy, M., Jackson, J., 2001. Migration of activity within normal fault systems: examples from the Quaternary of mainland Greece. *Journal of Structural Geology* 23, 489–506.
- Goldsworthy, M., Jackson, J., Haines, J., 2002. The continuity of active fault systems in Greece. *Geophysical Journal International* 148, 596–618.
- Hancock, P.L., Barka, A.A., 1987. Kinematic indicators on active normal faults in western Turkey. *Journal of Structural Geology* 9, 573–584.
- Hellenic Army Geographical Service, 1978. 1:250,000 Map Sheet “Khalkis”.
- Hellenic Army Geographical Service, 1992. 1:50,000 Map Sheet “Elefsis”. IGME, 1989. Seismotectonic map of Greece with seismological data. Scale 1:500,000.
- Katsikatos, G., 1977. La structure tectonique d’Attique et l’île d’Eubée. Proc. Vth Coll. on the Aegean Region, Athens. IGME Publications 1, pp. 211–228.
- Katsikatos, G., Mettos, A., Vidakis, M., Dounas, A., 1986. Geological Map of Greece (IGME series), Athinaï–Elefsis Sheet.
- King, G.F., Stein, R.S., Rundle, J.B., 1988. The growth of geological structures by repeated earthquakes. 1. Conceptual framework. *Journal of Geophysical Research* 93, 13307–13318.
- Kiratzi, A.A., 2002. Stress tensor inversions along the westernmost North Anatolian Fault Zone and its continuation into the North Aegean Sea. *Geophysical Journal International* 151, 360–376.
- Koukouvelas, I.K., Stamatopoulos, L., Katsanopoulou, D., Pavlides, S., 2001. A palaeoseismological and geoarchaeological investigation of the Eliki fault, Gulf of Corinth, Greece. *Journal of Structural Geology* 23, 531–543.
- Louis, I.F., Raftopoulos, D., Goulis, I., Louis, F.I., 2002. Geophysical imaging of faults and fault zones in the urban complex of Ano Liosia Neogene basin, Greece: synthetic simulation approach and field investigations. *International Conference on Earth Sciences and Electronics–2002 (ICESE–2002)*, pp. 269–285.
- Marinos, G., Katsikatos, G., Georgiades–Dikeoulia, E., Mirkou, R., 1971. The Athens’ schists formation. I. Stratigraphy and structure. *Annales Géologiques des Pays Helléniques* 23, 183–216.
- Mettos, A., Ioakim, Ch., Rondoyanni, Th., 2000. Palaeoclimatic and palaeogeographic evolution of Attica–Beotia (central Greece). *Geological Society of Greece Special Publication* 9, 187–196.
- Michetti, A.M., Ferrel, L., Esposito, E., Porfido, S., Blumetti, A.M., Vittori, E., Serva, L., Roberts, G.P., 2000. Ground effects during the 9 September 1998, Mw = 5.6, Lauria earthquake and the seismic potential of the “aseismic” Pollino Region in Southern Italy. *Seismological Research Letters* 71, 31–46.
- Morewood, N.C., Roberts, G.P., 2001. Comparison of surface slip and focal mechanism slip data along normal faults: an example from the eastern Gulf of Corinth, Greece. *Journal of Structural Geology* 23, 473–487.
- Pantosti, D., De Martini, P.M., Papanastassiou, D., Palyvos, N., Lemeille, F., Stavrakakis, G., 2001. A reappraisal of the 1894 Atalanti earthquake surface ruptures, central Greece. *Bulletin of the Seismological Society of America* 91, 760–780.
- Papadopoulos, G.A., 2000. Historical earthquakes and tsunamis in the Corinth Rift, Central Greece. National Observatory of Athens, Institute of Geodynamics, Publ. No. 12, Athens, 128pp.
- Papadopoulos, G.A., Drakatos, G., Papanastassiou, D., Kalogeras, I., Stavrakakis, G., 2000. Preliminary results about the catastrophic earthquake of 7 September 1999 in Athens, Greece. *Seismological Research Letters* 71, 318–329.
- Papadopoulos, G.A., Ganas, A., Pavlides, S., 2002. The problem of seismic potential assessment: case study of the unexpected earthquake of 7 September 1999 in Athens, Greece. *Earth Planets Space* 54, 9–18.
- Papanikolaou, D.J., Mariolacos, I.D., Lekkas, E.L., Lozios, S.G., 1988. Morphotectonic observations on the Asopos Basin and the coastal zone of Oropos. Contribution to the Neotectonics of northern Attica. *Bulletin of the Geological Society of Greece* 20, 251–267.
- Papazachos, B.C., Kiratzi, A.A., Papaioannou, C.A., Panagiotopoulos, D.G., 1991. Average regional seismic strain release rates in the Patraikos–Saronikos Gulfs (central Greece) based on historical instrumental data. *Bulletin of the Geological Society of Greece* 25(3), 225–238.

- Pavlidis, S.B., Zouros, N.C., Zhongjing, F., Shaoping, C., Tranos, M.D., Chatzipetros, A.A., 1999. Geometry, kinematics, and morphotectonics of the Yanqing–Huailai active faults (northern China). *Tectonophysics* 308, 99–118.
- Pavlidis, S.B., Ganas, A., Papadopoulos, G.A., 2002. The fault that caused the Athens September 1999  $M_s = 5.9$  earthquake: field observations. *Natural Hazards* 27, 61–84.
- Pomonis, A., 2002. The mount Parnitha (Athens) earthquake of September 7, 1999: a disaster management perspective. *Natural Hazards* 27, 171–199.
- Roberts, G.P., Ganas, A., 2000. Fault-slip directions in central and southern Greece measured from striated and corrugated fault planes: comparison with focal mechanism and geodetic data. *Journal of Geophysical Research* 105, 23443–23462.
- Robertson, A.H.F., Clift, P.D., Degnan, P.J., Jones, G., 1991. Tectonic evolution of the Mesozoic–Cenozoic Pindos Ocean: Greece. *Bulletin of the Geological Society of Greece* 25(1), 55–64.
- Sargeant, S.L., Burton, P.W., Douglas, A., Evans, J.R., 2002. The source mechanism of the Athens earthquake, September 7, 1999, estimated from P seismograms recorded at long range. *Natural Hazards* 27, 35–45.
- Stewart, I.S., Hancock, P.L., 1988. Normal fault zone evolution and fault scarp degradation in the Aegean region. *Basin Research* 1, 139–153.
- Stewart, I.S., Hancock, P.L., 1991. Scales of structural heterogeneity within neotectonic normal fault zones in the Aegean region. *Journal of Structural Geology* 13, 191–204.
- USGS (Athens earthquake solution; last accessed November 26, 2003), [http://neic.usgs.gov/neis/bulletin/99\\_EVENTS/990907115650/index.html](http://neic.usgs.gov/neis/bulletin/99_EVENTS/990907115650/index.html).